Computer Physics Communications 63 (1991) 84–94
North-Holland

Visualizing quantum scattering on the CM-2 supercomputer

John L. Richardson [1]

Thinking Machines Corporation, 245 First Street, Cambridge, MA 02142-1214, USA

Received 2 February 1990

We implement parallel algorithms for solving the time-dependent Schrödinger equation on the CM-2 supercomputer. These methods are unconditionally stable as well as unitary at each time step and have the advantage of being spatially local and explicit. We show how to visualize the dynamics of quantum scattering using techniques for visualizing complex wave functions. Several scattering problems are solved to demonstrate the use of these methods.

1. Introduction

Numerical solutions to the time-dependent Schrödinger equation have long been a challenging computational physics problem. In order to have good numerical solutions, it is necessary to have both a stable and a unitary algorithm. Methods which possess these desired properties are computationally quite expensive [1–3]. Here we use new techniques [4] that are unitary, explicit and local, as well as computationally simple. These techniques are implemented on the CM-2 supercomputer [6] and selected quantum-scattering problems are solved numerically and visualized.

Consider the time dependent Schrödinger equation in N-dimensional Euclidean space $\mathbb{R}^N$,

$$\mathrm{i}\hbar \frac{\partial}{\partial t} \Psi(\boldsymbol{x}, t) = \hat{H} \Psi(\boldsymbol{x}, t), \tag{1}$$

where $\hat{H}$ is the self-adjoint Hamiltonian operator for the system under study and $\Psi(\boldsymbol{x}, t)$ is the system's wave function. This evolution equation constrains $\int |\Psi(\boldsymbol{x}, t)|^2 \, \mathrm{d}^N \boldsymbol{x}$ to be time independent. For the special case of a single particle moving in a fixed potential field $V(\boldsymbol{x})$, the Hamiltonian for the system takes the form

$$\hat{H} = -\frac{\hbar^2}{2m} \nabla^2 + V(\boldsymbol{x}). \tag{2}$$

Given the initial wave function $\Psi_0(\boldsymbol{x}) = \Psi(\boldsymbol{x}, t_0)$, we would like to find Ψ at later times $t > t_0$. The formal solution to eq. (1) is given by

$$\Psi(\boldsymbol{x}, t) = \left(\exp\left(-\mathrm{i} \frac{(t - t_0)}{\hbar} \hat{H} \right) \Psi_0 \right)(\boldsymbol{x}, t). \tag{3}$$

To evaluate eq. (3), one needs an accurate way to evaluate the unitary action of $\exp(-\mathrm{i}(\Delta t/\hbar)\hat{H})$ on a state vector. Naive approaches that approximate the exponential by using the leading terms of the series expansion

$$\exp\left(-\mathrm{i} \frac{\Delta t}{\hbar} \hat{H} \right) = 1 - \mathrm{i} \frac{\Delta t}{\hbar} \hat{H} + \mathcal{O}\left(\left[\frac{\Delta t}{\hbar} \hat{H} \right]^2 \right) \tag{4}$$

[1] Email: john @ think.com.

0010-4655/91/$03.50

are unstable and are not unitary. Indeed, one finds after a very small number of iterations that the solution is dominated by high-frequency noise.

Other stable approaches that respect unitarity [1], such as Cayley's fractional form

$$\exp\left(-\mathrm{i}\frac{\Delta t}{\hbar}\hat{H}\right) = \left(1-\mathrm{i}\frac{\Delta t}{2\hbar}\hat{H}\right)\left(1+\mathrm{i}\frac{\Delta t}{2\hbar}\hat{H}\right)^{-1} + \mathcal{O}\left(\left[\frac{\Delta t}{\hbar}\hat{H}\right]^3\right) \tag{5}$$

work quite well, but are computationally expensive due to the large system of equations that must be solved in order to implement the inverse operator $[1 + \mathrm{i}(\Delta t/2\hbar)\hat{H}]^{-1}$ acting on a state vector at each time step.

Spectral-like methods [2] that write $\hat{H} = \hat{T} + \hat{V}$ where $\hat{T}$ is diagonal in Fourier space, and evaluate [#1]

$$\exp\left(-\mathrm{i}\frac{\Delta t}{\hbar}\hat{H}\right) = \exp\left(-\mathrm{i}\frac{\Delta t}{\hbar}\hat{T}\right)\exp\left(-\mathrm{i}\frac{\Delta t}{\hbar}\hat{V}\right) + \mathcal{O}\left(\left[\frac{\Delta t}{\hbar}\hat{H}\right]^2\right), \tag{6}$$

are stable and indeed unitary, but require a non-local Fourier transform and its inverse to evaluate $\exp[-\mathrm{i}(\Delta t/\hbar)\hat{T}]$ on a state vector.

Alternating direction implicit (ADI) methods have also been studied [3]. Although these methods are stable and unitary, they require multiple solutions to tridiagonal systems of equations at each time step.

2. Space splitting

Methods used here are based on splitting the kinetic operator $\hat{T}$ into a sum of M pieces such that $\hat{T} = \sum_{l=1}^{M}\hat{T}_l$. Each $\hat{T}_l$ is chosen so that it can be easily exponentiated. This can be accomplished by requiring each $\hat{T}_l$ to be the direct sum of matrices each of which is no larger than some modest size (we use 2 by 2) that is easy to exponentiate. The time-stepping operator is evaluated as [#2]

$$\exp\left(-\mathrm{i}\frac{\Delta t}{\hbar}\hat{H}\right) = \left(\prod_{l=1}^{M}\exp\left(-\mathrm{i}\frac{\Delta t}{\hbar}\hat{T}_l\right)\right)\exp\left(-\mathrm{i}\frac{\Delta t}{\hbar}\hat{V}\right) + \mathcal{O}\left(\left[\frac{\Delta t}{\hbar}\hat{H}\right]^2\right). \tag{7}$$

We shall show that this method is not only stable and unitary, but by construction it is also spatially local. For a large class of discretizations $\hat{T}$ can be divided into into M distinct parts. Whenever the line graph [#3] of the matrix of $\hat{T}$ can be M-colored, this is indeed the case [5]. These space-splitting methods are therefore applicable to unstructured or irregular grid problems.

To see how this works on a simple one-dimensional problem, consider a one-dimensional periodic system on a discrete spatial lattice with an even number L, of equally spaced sites and a uniform lattice spacing a. A second order approximation to the Laplacian leads to

$$(\hat{T}\Psi)_n = \frac{\hbar^2}{2ma^2}[2\Psi_n - \Psi_{n-1} - \Psi_{n+1}], \tag{8}$$

[#1] The Trotter product formula states that $\lim_{n\to\infty}[\exp(\mathrm{i}\hat{A}/n)\exp(\mathrm{i}\hat{B}/n)]^n = \exp[\mathrm{i}(A+B)]$.

[#2] To extend eq. (7) to an accuracy of $\mathcal{O}([\Delta t]^3)$ one can verify that $\exp[-\mathrm{i}(\Delta t/\hbar)\hat{H}] = (\prod_{l=1}^{M}\exp[-\mathrm{i}(\Delta t/2\hbar)\hat{T}_l])\times\exp[-\mathrm{i}(\Delta t/\hbar)\hat{V}](\prod_{l=M}^{1}\exp[-\mathrm{i}(\Delta t/2\hbar)\hat{T}_l]) + \mathcal{O}([(\Delta t/\hbar)\hat{\mathrm{H}}]^3)$ which also applies to eq. (6) when $M = 1$.

[#3] The *line graph L(G)* of a graph G is the graph that associates a vertex with each edge of G and an edge for each edge pair of G which meet at a vertex of G.

where n is a site index which takes on the values $n = 0, 1, 2, \ldots, L-1$. The matrix for $\hat{T}$ is

$$[T] = \frac{\hbar^2}{2ma^2}\begin{bmatrix} 2 & -1 & 0 & \cdots & 0 & -1 \\ -1 & 2 & -1 & \cdots & \ddots & 0 \\ 0 & -1 & 2 & -1 & \ddots & 0 \\ \vdots & \ddots & \ddots & \ddots & \ddots & \vdots \\ 0 & \ddots & \ddots & -1 & 2 & -1 \\ -1 & 0 & \cdots & 0 & -1 & 2 \end{bmatrix}, \tag{9}$$

which may be split into two parts [#4]. This splitting is chosen so that each independent piece may easily be exponentiated. Our choice is

$$[T_{\text{even}}] = \frac{\hbar^2}{2ma^2}\begin{bmatrix} 1 & -1 & 0 & 0 & \cdots & 0 & 0 \\ -1 & 1 & 0 & 0 & \ddots & \ddots & \vdots \\ 0 & 0 & 1 & -1 & 0 & \ddots & \vdots \\ 0 & 0 & -1 & 1 & 0 & \ddots & \vdots \\ \vdots & \ddots & \ddots & \ddots & \ddots & 0 & 0 \\ 0 & \ddots & \ddots & \ddots & 0 & 1 & -1 \\ 0 & \cdots & \cdots & \cdots & 0 & -1 & 1 \end{bmatrix}, \tag{10}$$

and

$$[T_{\text{odd}}] = \frac{\hbar^2}{2ma^2}\begin{bmatrix} 1 & 0 & 0 & 0 & \cdots & 0 & -1 \\ 0 & 1 & -1 & 0 & \ddots & \ddots & 0 \\ 0 & -1 & 1 & 0 & \ddots & \ddots & \vdots \\ \vdots & \ddots & \ddots & \ddots & \ddots & \ddots & \vdots \\ 0 & \ddots & \ddots & 0 & 1 & -1 & \vdots \\ 0 & \ddots & \ddots & 0 & -1 & 1 & 0 \\ -1 & \cdots & \cdots & \cdots & \cdots & 0 & 1 \end{bmatrix}. \tag{11}$$

Both T_{even} and T_{odd} are direct sums of the 2 by 2 matrix

$$M = \frac{\hbar^2}{2ma^2}\begin{bmatrix} 1 & -1 \\ -1 & 1 \end{bmatrix}$$

which may easily be exponentiated, since

$$\exp\left(-\mathrm{i}\frac{\Delta t}{\hbar}\hat{M}\right) = 1 + [\exp(-\mathrm{i}\epsilon) - 1]\frac{ma^2}{\hbar^2}M = \frac{1}{2}\begin{bmatrix} 1+\exp(-\mathrm{i}\epsilon) & 1-\exp(-\mathrm{i}\epsilon) \\ 1-\exp(-\mathrm{i}\epsilon) & 1+\exp(-\mathrm{i}\epsilon) \end{bmatrix} = \begin{bmatrix} \alpha & \beta \\ \beta & \alpha \end{bmatrix}, \tag{12}$$

where $\epsilon = \Delta t\hbar/\mathrm{m}a^2$ and $\alpha = [1 + \exp(-\mathrm{i}\epsilon)]/2$ and $\beta = [1 - \exp(-\mathrm{i}\epsilon)]/2$. Of course $\exp[-\mathrm{i}(\Delta t/\hbar)\hat{M}]$ is unitary with eigenvalues $\lambda_1 = 1$ and $\lambda_2 = \exp(-\mathrm{i}\epsilon)$.

[#4] The line graph of an even 1-torus is again an even 1-torus which can be 2-colored by associating the even and odd vertices.

These relations may also be stated algebraically as

$$\left(\hat{T}_{\text{even}}\Psi\right)_n = \frac{\hbar^2}{2ma^2}\left(\Psi_n - \frac{1-(-1)^n}{2}\Psi_{n-1} - \frac{1+(-1)^n}{2}\Psi_{n+1}\right) \tag{13}$$

and

$$\left(\hat{T}_{\text{odd}}\Psi\right)_n = \frac{\hbar^2}{2ma^2}\left(\Psi_n - \frac{1+(-1)^n}{2}\Psi_{n-1} - \frac{1-(-1)^n}{2}\Psi_{n+1}\right). \tag{14}$$

The exponentiated forms are

$$\left[\exp\left(-\mathrm{i}\frac{\Delta t}{\hbar}\hat{T}_{\text{even}}\Psi\right)\right]_n = \alpha\Psi_n - \beta\frac{1-(-1)^n}{2}\Psi_{n-1} - \beta\frac{1+(-1)^n}{2}\Psi_{n+1} \tag{15}$$

and

$$\left[\exp\left(-\mathrm{i}\frac{\Delta t}{\hbar}\hat{T}_{\text{odd}}\Psi\right)\right]_n = \alpha\Psi_n - \beta\frac{1+(-1)^n}{2}\Psi_{n-1} - \beta\frac{1-(-1)^n}{2}\Psi_{n+1}. \tag{16}$$

The unitarity of the algorithm implies that the time advanced norms of $|\exp[-\mathrm{i}(\Delta t/\hbar)\hat{T}_{\text{even}}\Psi]|^2$, $|\exp[-\mathrm{i}(\Delta t/\hbar)\hat{T}_{\text{odd}}\Psi]|^2$ and $|\exp[-\mathrm{i}(\Delta t/\hbar)\hat{V}\Psi]|^2$ are left unchanged and equal to the norm of $|\Psi|^2$ at the beginning of the time step, so the algorithm is *unconditionally stable*.

Although we have used a second-order approximation to the Laplacian operator for demonstration purposes, there is no reason why higher-order approximations may not be used. For example, a fourth-order approximation [#5] leads to a $\hat{T}$ which can be split into four parts. The four parts are the even and odd connections to nearest-neighbor sites as in the quadratic case and the additional even and odd connections to next to nearest neighboring sites.

All of these one-dimensional equations generalize to N spatial dimensions. In N spatial dimensions the site index n is replaced by a vector $\boldsymbol{n} = [n_1, n_2, \ldots, n_N]$ and the quadratic approximation to the kinetic operator T becomes

$$(\hat{T}\Psi)_{\boldsymbol{n}} = \frac{\hbar^2}{2ma^2}\left[2N\Psi_{\boldsymbol{n}} - \sum_{a=1}^{N}\left(\Psi_{\boldsymbol{n}-\hat{\boldsymbol{e}}_a} + \Psi_{\boldsymbol{n}+\hat{\boldsymbol{e}}_a}\right)\right], \tag{17}$$

where $\hat{\boldsymbol{e}}_a$ is a unit vector in the ath direction and each component $n_a = \hat{\boldsymbol{e}}_a \cdot \boldsymbol{n}$ of $\boldsymbol{n}$ takes n the values $n_a = 0, 1, \ldots, L_a - 1$. Here $\hat{T}$ may be split up into $2N$ parts, or $\hat{T} = \sum_{a=1}^{N}(\hat{T}^a_{\text{even}} + \hat{T}^a_{\text{odd}})$. As in the one-dimensional case, we find that on the N-torus

$$\left(\exp\left[-\mathrm{i}\frac{\Delta t}{\hbar}\hat{T}^a_{\text{even}}\right]\Psi\right)_{\boldsymbol{n}} = \alpha\Psi_{\boldsymbol{n}} - \beta\frac{1-(-1)^{\sum_{b=1}^{N} n_b}}{2}\Psi_{\boldsymbol{n}-\hat{\boldsymbol{e}}_a} - \beta\frac{1+(-1)^{\sum_{b=1}^{N} n_b}}{2}\Psi_{\boldsymbol{n}+\hat{\boldsymbol{e}}_a} \tag{18}$$

and

$$\left(\exp\left[-\mathrm{i}\frac{\Delta t}{\hbar}\hat{T}^a_{\text{odd}}\right]\Psi\right)_{\boldsymbol{n}} = \alpha\Psi_{\boldsymbol{n}} - \beta\frac{1+(-1)^{\sum_{b=1}^{N} n_b}}{2}\Psi_{\boldsymbol{n}-\hat{\boldsymbol{e}}_a} - \beta\frac{1-(-1)^{\sum_{b=1}^{N} n_b}}{2}\Psi_{\boldsymbol{n}+\hat{\boldsymbol{e}}_a} \tag{19}$$

[#5] $(\hat{T}\Psi)_n = (\hbar^2/24ma^2)[30\Psi_n - 16\Psi_{n-1} - 16\Psi_{n+1} + \Psi_{n-2} + \Psi_{n+2}] + \mathcal{O}(a^4)$.

[#6] By construction, each $\hat{T}_l$ is the direct sum of 2 by 2 and 1 by 1 matrices.

The unconditional stability argument given for the one-dimensional case depends only on the unitarity of the algorithm and therefore is again applicable in the N-dimensional case.

These results for the N-torus may also be extended to arbitrary grids (structured or unstructured) with different topologies. As mentioned earlier, once the line graph of $\hat{T}$ has been M-colored, the M operators $\hat{T}_l$, $l = 1, 2, \ldots, M$, are easy to exponentiate [#6] and the evolution operator is again unitary, extending the previous results.

The stability results for the Schrödinger equation also apply to the diffusion equation. The simple substitutions $t \to -\mathrm{i}t$ and $\Delta t \to -\mathrm{i}\Delta t$ with $V = 0$ in all our previous formula transforms the quantum mechanical Schrödinger equation into the classical diffusion equation. All of the operators that were previously unitary in the Schrödinger case now become real operators with positive eigenvalues that are all less than or equal to unity, so unconditional stability again applies.

3. Visualizing wave functions

In order to *see* the quantum scattering process, we need a technique to look at the evolution of complex wave functions. Standard probability-density plots can be viewed, but there is a wealth of additional information contained in the phase of the wave function. We desire a technique to vew *both* the *amplitude* and the *phase* of the wave function simultaneously. Most of us have some sort of metal image when we are presented with the concepts of a *pole*, a *zero*, a *branch point* or a *branch cut*. Most graphical techniques for describing complex functions are quite crude in that poles and zeros may be represented by $\times$'s and O's and branch cuts identified by thick lines, but detailed phase information is usually lost as well as pole and zero multiplicity data. Here we propose a standard for displaying complex functions that uses color to convey intensity and phase information.

3.1. Projecting into color

Color space is a compact three-dimensional space, and a point in the space can be uniquely specified by the three intensities (r, g, b) that represent the intensity of the red, green and blue electron guns in a color display tube. The intensities r, g and b each lie in the interval [0,1]. The eight vertices of the color cube are displayed in fig. 1. The color intensities vary linearly between all points in the cube.

To visualize a complex number $z = x + \mathrm{i}y$ or a two-dimensional vector field (v_1, v_2), we must find a mapping from $\mathbb{C}$ or equivalently $\mathbb{R}^2$ into the color cube $[0,1]^3$. There are an infinite number of possible mappings to choose from.

One well known mapping stereographically maps the complex plane onto the surface of the unit sphere S^2 by finding the intersection of the ray that passes through the north pole (0, 0, 1) and the point in the plane $(x, y, 0)$. Points that lie inside the unit circle in the complex plane are mapped to the southern hemisphere and the origin $z = 0$ is mapped to the south pole (0, 0, -1). Points that lie outside the unit circle are mapped to the northern hemisphere and all points at ∞ are mapped to the north pole (0, 0, 1). Points on the unit circle map directly to the equator. This mapping is defined by

$$(x', y', z') = \frac{(2x, 2y, x^2 + y^2 - 1)}{x^2 + y^2 + 1} \tag{20}$$

and this projection is shown in fig. 2.

One natural way to imbed the unit sphere in the color tube is by shrinking its radius to 1/2 and placing

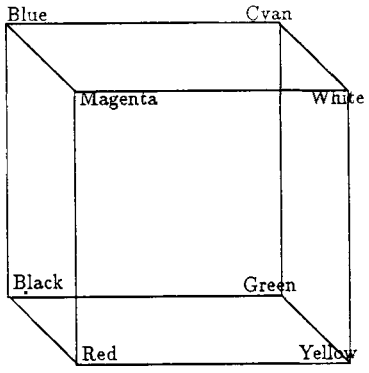

Fig. 1. The color cube.

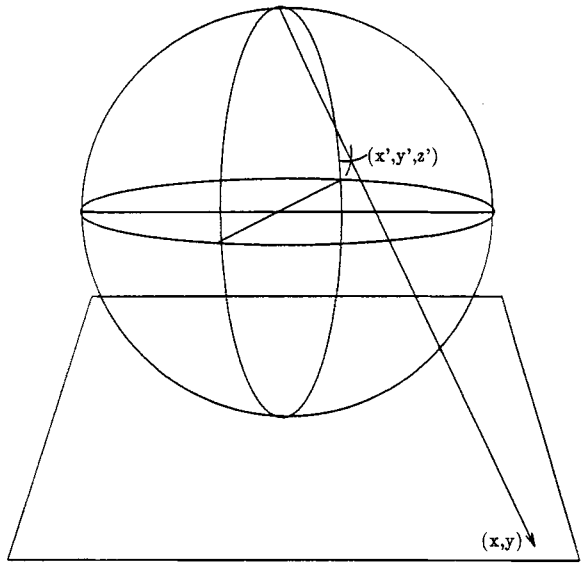

Fig. 2. Stereographic projection of the complex plane onto the surface of the unit sphere.

the center of the sphere at the center of the color cube $(r, g, b) = (1/2, 1/2, 1/2)$. We align the southern to northern axis of the sphere along the ray from (0, 0, 0) to (1, 1, 1) in the color cube. This orientation is chosen so that the south pole is as close to black (0, 0, 0) as possible (aesthetically zeroes which have no amplitude ought to the black) and the north pole is as close to white (1, 1, 1) as possible (likewise poles which have enormous amplitudes ought to be white). The azimuthal orientation will be uniquely determined if we require that the positive real axis has maximal red intensity (R is for real or right or red!).

This map looks quite reasonable on the unit circle but the intensities at the origin and ∞ are not distinct enough. This is because a sphere of radius $1/2$ can only have points that are a fraction $1/\sqrt{3}$ or about 58% of the distance to the corners at (0, 0, 0) and (1, 1, 1) which leads to weak intensities. Intensities for poles are not bright enough and zeros are not dark enough. To remedy this situation we will replace each hemisphere of the sphere by separate cones whose vertices are at (0, 0, 0) and (1, 1, 1) and whose bases lie on the equator. In a coordinate system where the z-axis is the axis of the cones, this mapping is defined by:

$$(x', y', z') = \frac{\left(2x, 2y, \eta\left(x^2+y^2-1\right)\sqrt{3}\left(x^2+y^2+1-2\sqrt{x^2+y^2}\right)\right)}{x^2+y^2+1}, \tag{21}$$

where

$$\eta(t) = \begin{cases} 1, & t > 0, \\ -1, & t < 0. \end{cases}$$

If we rescale eq. (21) by a factor of $1/2$, followed by a rotation to align the cones axis with the diagonal of the color cube and follow this by a translation to the center of the color cube we find:

$$r = \tfrac{1}{2} + \eta\left(x^2+y^2-1\right)\left(\frac{1}{2} - \frac{\sqrt{x^2+y^2}}{1+x^2+y^2}\right) + \frac{2x}{\sqrt{6}\left(1+x^2+y^2\right)}, \tag{22}$$

$$g = \tfrac{1}{2} + \eta\left(x^2+y^2-1\right)\left(\frac{1}{2} - \frac{\sqrt{x^2+y^2}}{1+x^2+y^2}\right) - \frac{x}{\sqrt{6}\left(1+x^2+y^2\right)} + \frac{y}{\sqrt{2}\left(1+x^2+y^2\right)}, \tag{23}$$

$$b = \tfrac{1}{2} + \eta\left(x^2+y^2-1\right)\left(\frac{1}{2} - \frac{\sqrt{x^2+y^2}}{1+x^2+y^2}\right) - \frac{x}{\sqrt{6}\left(1+x^2+y^2\right)} - \frac{y}{\sqrt{2}\left(1+x^2+y^2\right)}. \tag{24}$$

These completely define our mappings from the complex plane into the color cube. This map has the desired properties at poles and zeros and will be used for visualizing complex wave functions in the next section.

4. Scattering examples

We have numerically studied the scattering of a Gaussian wave packet by a localized potential $V(x)$ using the CM-2 supercomputer. These algorithms are very easy to program using CMFortran as can be seen by the following time-stepping routine.

```
c  Time stepping subroutine for two dimensional
c  Schrödinger equation

   SUBROUTINE step(psi,alpha,betaeven,betaodd,expv,count)
   PARAMETER(n=1024)
   COMPLEX psi(n,n),alpha,betaeven(n,n),betaodd(n,n),expv(n,n)
   INTEGER i,count

   DO i=1,count

   psi=expv*psi

   psi=alpha*psi+betaeven*CSHIFT(psi,DIM=1,SHIFT=-1)
  &              +betaodd *CSHIFT(psi,DIM=1,SHIFT=+1)
   psi=alpha*psi+betaeven*CSHIFT(psi,DIM=1,SHIFT=+1)
  &              +betaodd *CSHIFT(psi,DIM=1,SHIFT=-1)

   psi=alpha*psi+betaeven*CSHIFT(psi,DIM=2,SHIFT=-1)
  &              +betaodd *CSHIFT(psi,DIM=2,SHIFT=+1)
   psi=alpha*psi+betaeven*CSHIFT(psi,DIM=2,SHIFT=+1)
  &              +betaodd *CSHIFT(psi,DIM=2,SHIFT=-1)

   END DO

   RETURN
   END
```

This is a very simple minded, but easy to understand subroutine. The array expv( ) is $\exp[-i(\Delta t/\hbar)\hat{V}]$ and the arrays betaeven( ) and betaodd( ) are defined to be zero on odd or even sites respectively and β

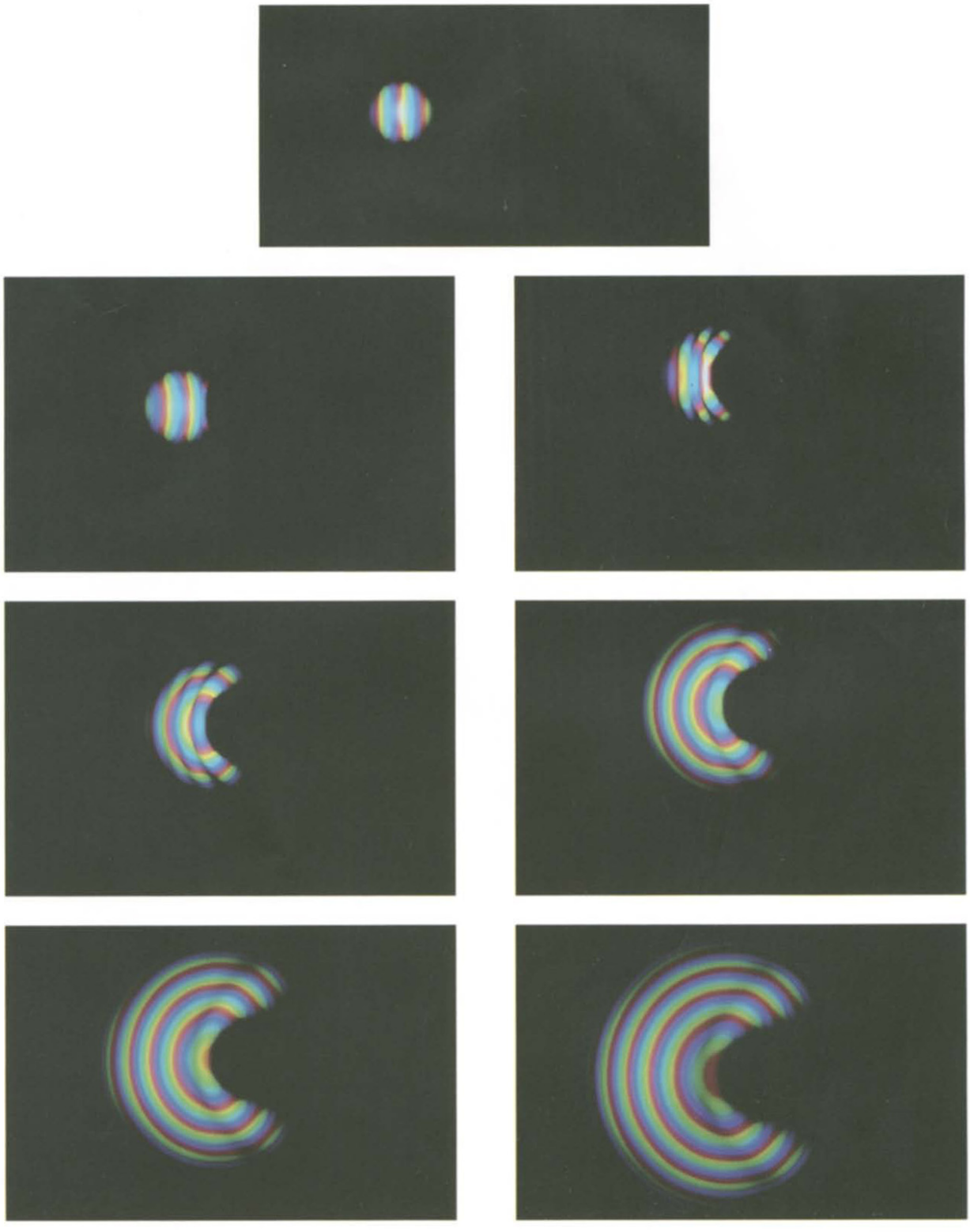

Color plate 1. A packet scattered from a repulsive (positive) potential.

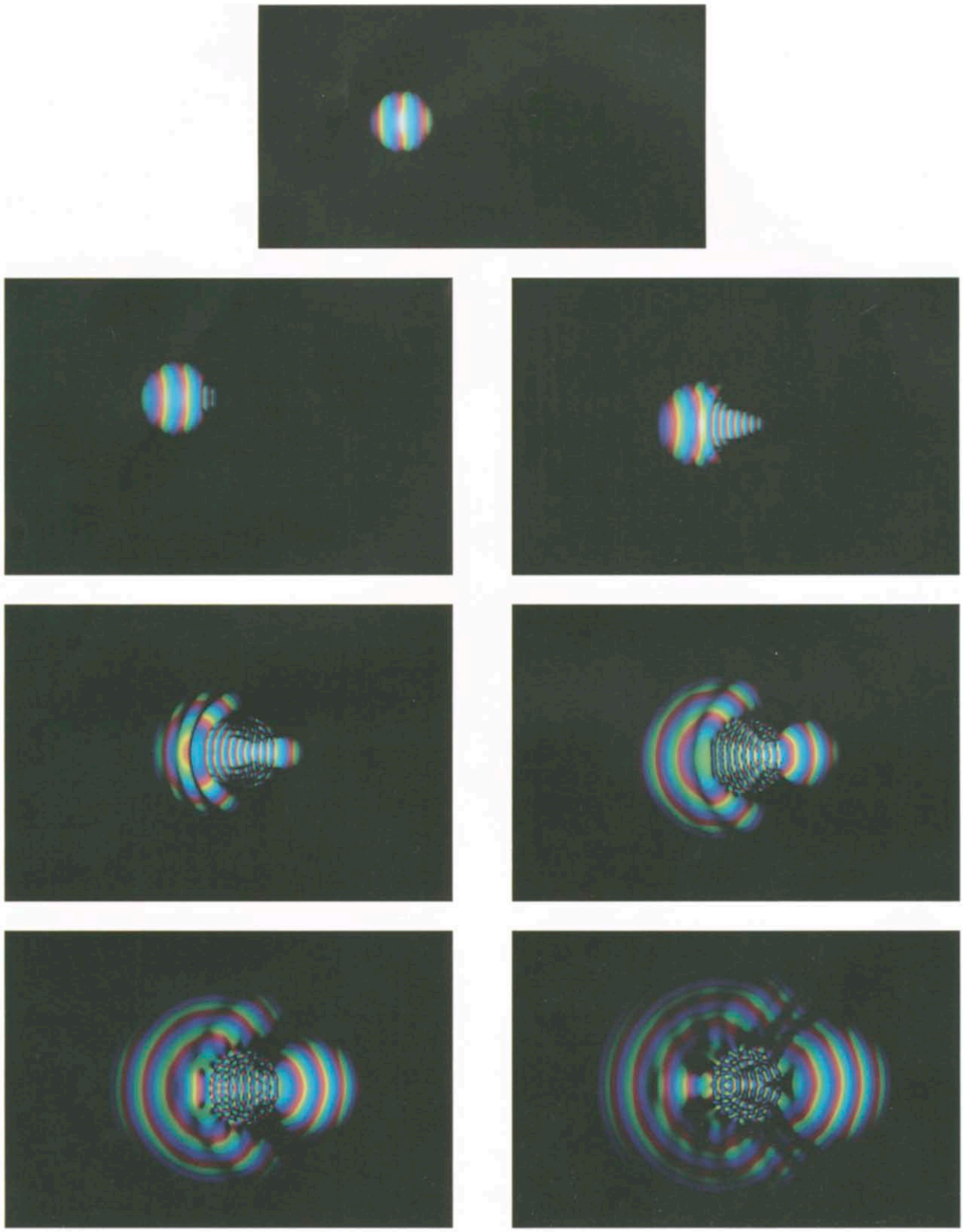

Color plate 2. A packet scattered from an attractive (negative) potential.

otherwise. This implementation does unnecessary multiplications by zero but still manages to run at about 800 Mflops on a 64K CM-2. A more efficient CMFORTRAN version runs at above 2000 Mflops on the same hardware [7].

Given an initial wave function described by

$$\Psi(x, 0) = \left(2\pi(\Delta x)^2\right)^{N/2} \exp\left(- \frac{(x - x_0)^2}{2(\Delta x)^2} + \mathrm{i}\, p \cdot x \right) \tag{25}$$

centered at the point x_0 and moving with momenta p, we would like to observe the time evolution $\Psi(x, t)$ of the scattering process.

We will restrict ourselves to two spatial dimensions so that the results can be seen on the sheets of this paper. In order to visualize the *complex* wave function, we have used the technique described in the previous section.

Color plate 1 shows a sequence of frames where a packet is scattered from a repulsive (positive) potential that is constant inside a circle of radius r_0. Notice the de Broglie waves perpendicular to the direction of motion in the initial Gaussian wave packet as it move to the right. As the packed moves it spreads and finally it contacts the repulsive potential and is reflected by it. The wave function is repelled by the potential.

Color plate 2 shows a sequence of frames where a packet is scattered from an attractive (negative) potential that is constant inside a circle of radius r_0. Notice how the wave function is attracted by the potential which seems to pull it through the scattering center causing a peak in the forward scattering cross section.

These frames can be computed and viewed continuously using the CM-2 supercomputer, and vidieotapes of scattering phenomena have been made by the author [9].

5. Conclusion and generalizations

We have implemented new algorithms for the numerical integration of the time-dependent Schrödinger equation using the CM-2 and demonstrated their use. The algorithms are unconditionally stable, local unitary, explicit and are easy to implement. In addition we have introduced new visualization techniques for complex functions or two-dimensional vector fields.

We have also shown how to extend these integration algorithms to unstructured grids and to simulate diffusion processes.

As one might anticipate from our discussion, these space-splitting techniques are quite general and have been extended to a broader class of wave phenomena including electromagnetic processes, fluid fluid flow and mechanical phenomena [8].

Acknowledgements

I would like thank Art Williams and Denny Dahl of Thinking Machines Corporation for many fruitful discussions and the referee of this article for pointing out the detailed work contained in ref. [4] whose methods had been independently discovered by the present author.

References

[1] A. Goldberg, H.M. Schey and J.L. Schwartz, Am. J. Phys. 35 (1967) 177.
[2] R.H. Hardin and F.D. Tappert, SIAM Rev. 15 (1973) 423.

[3] I. Galbraith, Y.S. Ching and E. Abraham, Am. J. Phys. 52 (1984) 60.
[4] H. DeRaedt, Comput. Phys. Rep. 7 (1987) 1.
[5] F. Harary, Graph Theory (Addison-Wesley, Reading, MA, 1971) p. 71.
[6] CM-2 Technical Summary, Thinking Machines Corporation, Cambridge, MA.
[7] A. Williams, private communication.
[8] J.L. Richardson, in preparation.
[9] Best of Visualization (video tape), Thinking Machines Corporation, Cambridge, MA.